# MEASUREMENT OF PROTON TUNNELLING IN SHORT HYDROGEN BONDS IN SINGLE CRYSTALS OF 3,5 PYRIDINECARBOXYLIC ACID USING NUCLEAR MAGNETIC RESONANCE SPECTROSCOPY

I. Frantsuzov[†,‡], S.J. Ford[#,ζ], I. Radosavljevic Evans[ζ], A.J. Horsewill[‡], H.P. Trommsdorff [#,ϒ], M.R. Johnson[#]

[‡]Department of Physics and Astronomy, University of Nottingham, Nottingham NG7 2RD, U.K.

[#]Institute Laue Langevin, BP 156, 38042 Grenoble, France

[ζ]Department of Chemistry, Durham University, Durham DH1 3LE, U.K.

[ϒ]University of Grenoble 1/CNRS, LIPhy UMR 5588, BP 87, 38041 Grenoble, France

## Abstract

In this letter, we present NMR spin-lattice and relaxometry data for proton transfer in one of the shortest known N-H···O hydrogen bonds in a single crystal of 3,5 pyridinedicarboxylic acid (35PDCA). It is widely believed that proton transfer by quantum tunnelling does not occur in short hydrogen bonds since the ground state energy level lies above the potential barrier yet this data shows a temperature independent, proton tunnelling rate below 77 K and a clear deviation from classical dynamics below 91 K. This study therefore suggests that proton tunnelling occurs in *all* hydrogen bonds at low temperature and the cross-over temperature to classical hopping must be determined when evaluating whether proton tunnelling persists at higher temperature, for example in enzyme catalysis under physiological conditions.

Hydrogen bonds (HB's) are ubiquitous in nature underpinning complex molecular architecture and reactions which involve proton transfer (PT). Studied for more than one hundred years [1] HB's have been of continuous interest in physics [2] chemistry [3,4,5] and biology [6]. In the latter case, the role of HB's in enzyme catalysis is widely studied. Cleland et al. [7] first proposed that short strong HB's play a key role in enzyme catalysis. While the strength of the HB's has been contested [8,9,10], short HB's with low barriers are considered essential in enhancing catalytic rates; protons being almost centred in short HB's are easily able to cross the low barrier from donor to acceptor atom [11]. Subsequently protein structures have been found which demonstrate the existence of such short HB's [12].

Proton tunnelling in longer HB's has also been shown to enhance the enzymatic rate through its non-classical dependence on the proton (H/D/T) mass – the kinetic isotope effect [13,14]. In addition, as demonstrated for simpler molecular systems [15,16,17], the coupling between large amplitude PT with small amplitude vibrations has been observed in enzymes by isotopic substitution of the molecular skeleton in the vicinity of the active HB's [18].

However, proton tunnelling in short HB's has never been demonstrated in the context of enzyme catalysis, or more generally in the fields of physics and chemistry.

Proton dynamics in HB's is typically described in an asymmetric, 1D, two-well potential where the abscissa is the tunnelling coordinate describing the proton position and the associated displacements in the molecular skeleton. Classical hopping over the central barrier, height $V$, separating the two wells is described as an Arrhenius process and the hopping rate is proportional to $exp(-(V-E_0)/kT)$ where $E_0$ is the ground state energy and $T$ is the temperature. The tunnelling rate for through barrier processes is proportional to $J^2$ where $J$ is the tunnelling matrix element proportional to $exp(-\sqrt{m(V-E_0)}a/\hbar)$, $m$ being the mass of the tunnelling particle and $a$ the separation of the potential wells. The classical hopping rate increases with $T$ whereas the tunnelling matrix element is independent of $T$ so that tunnelling processes dominate in the low $T$ limit. The cross-over between quantum and classical dynamics depends on $V$, occurring at lower $T$ for shorter HB's with smaller $V$ [19]. For the shortest HB's, it is generally assumed that tunnelling does not occur [20] since the barrier lies below the ground state energy level. However, a key parameter in this evaluation is the effective mass $m$ of the tunnelling particle, which depends on vibrations coupled to PT.

Given the uncertainty in calculating the potential energy surface, particularly for extended networks of inter-molecular HB's and evaluating the mass of the tunnelling particle, direct experimental

observation of tunnelling is of fundamental importance. In the case of benzoic acid, the PT rate has been measured directly by NMR relaxometry and quasi-elastic neutron scattering [21], revealing a constant, non-zero rate in the limit of low temperatures. Independently, coherent tunnelling was measured in this system through the doubling of the ground state level [22]. Incoherent tunnelling, via excited vibrational states, dominates the rate of PT at all temperatures since the potential barrier, estimated to be 2000 K [23], is always significantly greater than $kT$. However, in short HB's, the direct observation of tunnelling processes has, to our knowledge, never been reported despite many experimental [24,25,26,27,28] and theoretical [29, 30, 31,32 ,33,34,35,36] studies.

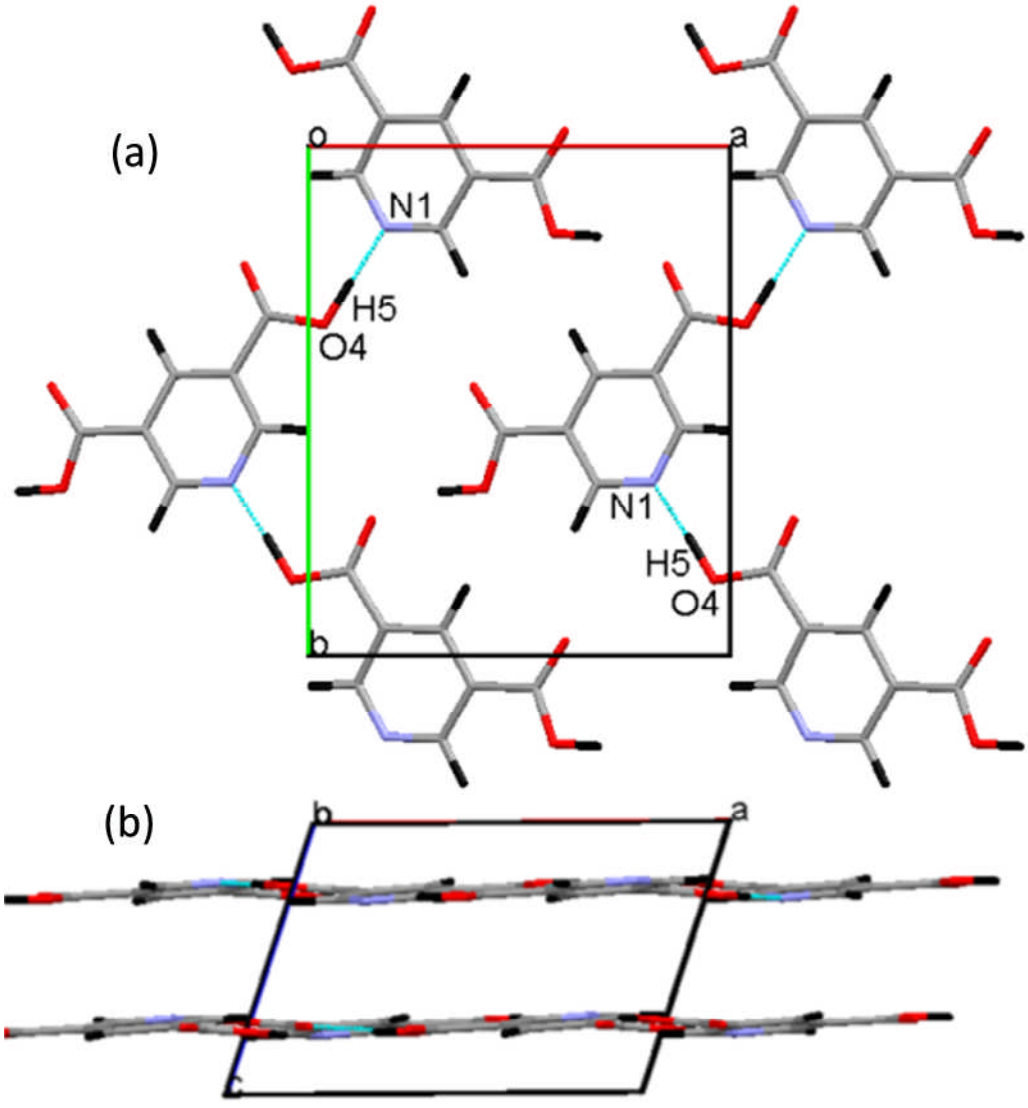


*Figure 1: Crystal structure of 35PDCA showing (a) the a-b plane and (c) the molecular sheets perpendicular to the c*-axis.*

3,5-pyridinedicarboxylic acid (35PDCA) is an almost perfect model system in which to study PT in a very short HB (Figure 1). The inter-molecular HB has a N-O distance of 2.54 Å and lies in the few % of

the shortest known N-H···O HB's [37,38]. The proton is almost centred and is clearly observed in neutron diffraction [39,40] to migrate from the donor N at low temperature to the acceptor O at room temperature. The proton jump distance is 0.1 Å in the protonated crystal and at 200 K the proton is, on average, centred. Since the proton migrates completely from donor to acceptor, the skeletal change accompanying PT can be estimated from the difference between low and high temperature structures. Linear interpolation between these structures, after rescaling the low temperature cell parameters to those of the room temperature crystal structure and optimising the internal atomic coordinates, allows the potential energy surface (PES) to be estimated using solid state, DFT methods [37,41,42,43]. Figure 2 shows, for the extreme structures and one intermediate structure, the 1D potential energy variation along the proton coordinate – they are cuts through the 2D PES [37]. Each 1D potential is a single asymmetric well but the potential energy variation along the straight line path between the extreme structures in the 2D PES displays a two-well potential due to the skeletal displacement. The PT distance is 0.3 Å because these calculations are based on the deuterated crystal structure.

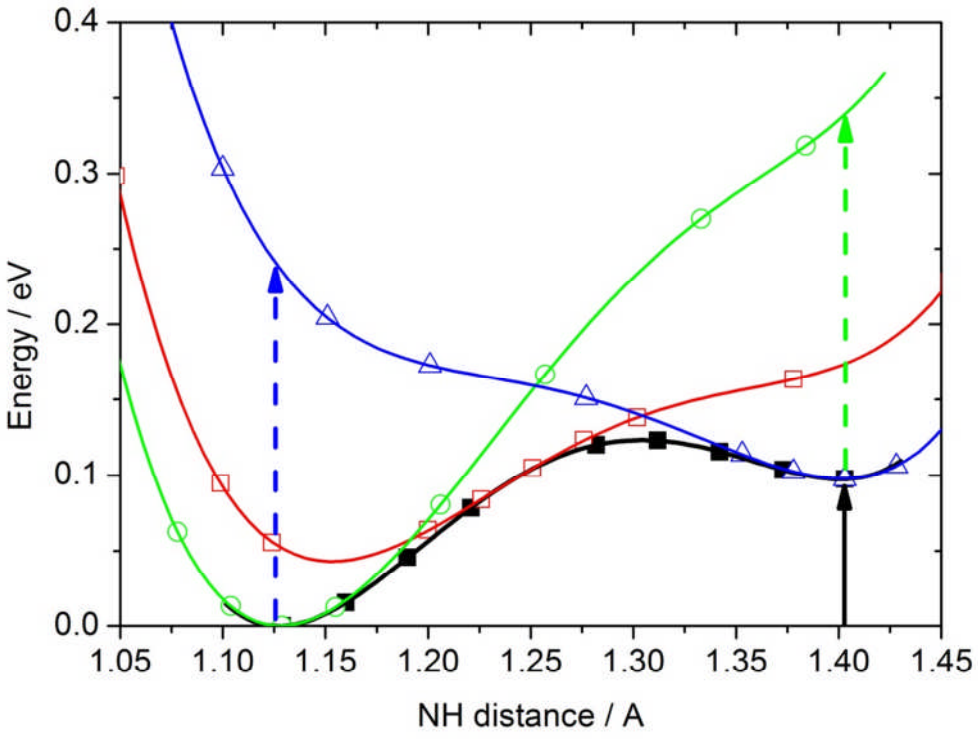


*Figure 2: Two-well potential along the linear path in the 2D PES (full squares). Single-well potentials obtained from 1D mapping (proton coordinate only) of the potential energy for the low (open circles) and high temperature (open triangles) structures and one intermediate structure (open squares). The solid black arrow indicates the energy cost of transferring 4 protons, including structural reorganisation (1140 K), the dashed arrows indicate the additional energy cost with the molecular skeleton fixed (2670 K).*

The two-well potential energy variation in Figure 2 is similar to the one calculated from a transition state (TS) search for the intra-molecular HB in benzoylacetone [12] for which the ground state level of the proton was estimated from the O-H stretch mode to lie above the barrier, excluding the possibility of quantum tunnelling. However this mode, with effective mass close to 1 amu, does not correspond to a TS potential for which all atoms are displaced. For 35PDCA, PT involves a significant electronic change ($NH^{\delta+}\cdots O^{\delta-} \rightarrow N\cdots HO$) and therefore a change of molecular geometry, so the tunnelling mass must be much higher than 1 amu. Diffraction data and solid state DFT calculations for 35PDCA therefore provide the framework for measuring quantum tunnelling in PT dynamics in one of the shortest known HB's.

PT has been investigated on a single crystal of fully-protonated 35PDCA using $^1$H spin-lattice relaxation as a function of magnetic **B**-field, $B_0$, and temperature $T$. The migrating $^1$H nucleus of the HB is physically close to the $^{14}$N atom on the donor molecule so modulation of the $^1$H-$^{14}$N dipolar interaction makes a significant contribution to the spin-lattice relaxation. The HB proton also experiences homo-nuclear dipolar interactions with other protons in the unit cell, including the immobile $^1$H nuclei on the phenyl ring. Dipolar interactions dominate over all other magnetic interactions in determining the $^1$H relaxation. Fluctuations in the magnetic interactions arising from the proton motion in the short HB are characterised by the correlation time, $\tau_c$.

Spin-lattice relaxation in 35PDCA is governed by the solutions of a pair of coupled differential equations corresponding to the $^{14}$N and $^1$H spin reservoirs [37,44,45,46,[47]]. Experimental observations and numerical modelling show that the $^1$H spin-lattice relaxation rate is closely approximated by the diagonal element of the relaxation matrix. Furthermore, the modulation of the hetero-nuclear $^{14}$N-$^1$H dipolar interaction dominates over $^1$H-$^1$H homo-nuclear interactions so the leading terms in the relaxation rate samples the spectral density at the $^1$H Larmor frequency $\omega_H=\gamma_H B_0$ and $2\omega_H$. Since $\omega_H$ is approximately 14 times the Larmor frequency of $^{14}$N, the $^1$H spin-lattice relaxation rate may be written in the following form,

$$\frac{1}{T_1^{(H)}(B_0,T)} \cong C_D K(T)[cL(\gamma_H B_0,\tau_c) + (1-c)L(2\gamma_H B_0,\tau_c)] \qquad (1)$$

where $\gamma_H$ is the $^1$H magnetogyric ratio, $L(\omega,\tau_c)=2\tau_c/(1+\omega^2\tau_c^2)$ is a Lorentzian with half-width at half-maximum equal to $\tau_c^{-1}$ and $c$ determines the ratio of the two Lorentzian components that sample the spectral density at $\omega_H$ and $2\omega_H$. The amplitude of the profile $1/T_1^{(H)}(B_0)$ is determined by the product $C_D K(T)$ where $C_D$ is a dipolar constant and $K(T)$ is a population factor dependent on temperature and the energy asymmetry of the two-well potential. With the field $B_0$ applied parallel to the $c^*$-axis, $C_D^{(calc)} = 6.50 \times 10^7\ s^{-2}$ and $c = 0.392$ were calculated from the crystal structure.

The $^{1}$H spin-lattice relaxation times $T_1^{(H)}$ were measured using a saturation-recovery pulse sequence. In order to determine the field dependence, $T_1^{(H)}(B_0)_T$, a field-cycling procedure was incorporated into this sequence [48,49]. In general, the proximity of the $^{14}$N nucleus to the migrating hydrogen renders the $^{1}$H spin-lattice relaxation bi-exponential although, in practice, the $^{1}$H polarisation-recovery curves displayed only small deviations from single exponential behaviour. However, $^{1}$H polarisation recovery was observed to systematically depend on the initial $^{14}$N state so, before measuring each point in the $^{1}$H polarisation-recovery curve, the initial $^{14}$N polarisation was prepared in the same way.

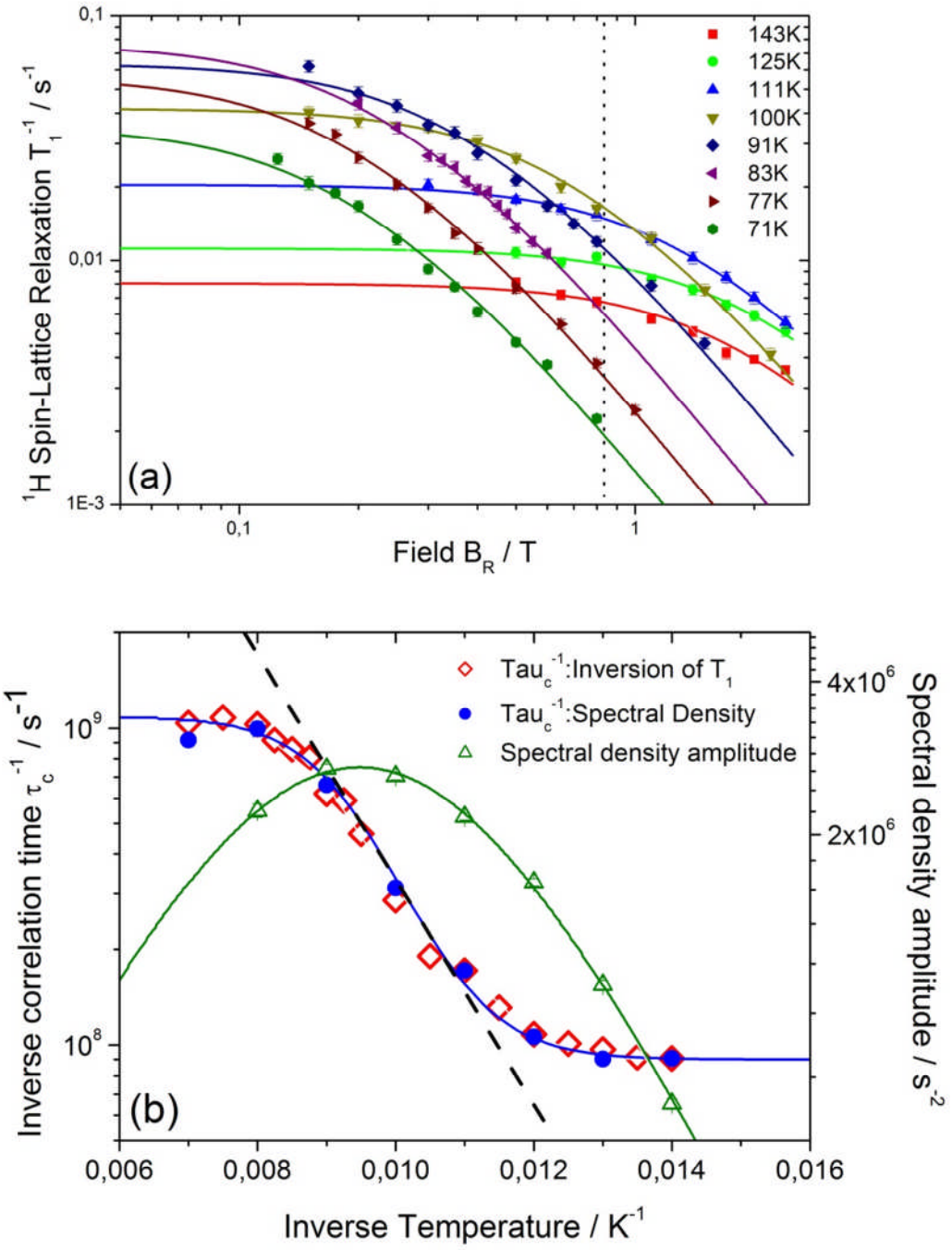


***Figure 3: (a) Spectral density profiles determined from the B-field dependence of the spin-lattice relaxation time. Solid curves are fits with Eqn. (1). The vertical dashed line denotes a fixed-field $T_1$ measurement [37]. (b) – left axis: Inverse temperature dependence of the PT correlation rate, $\tau_c^{-1}$. Solid symbols are determined from the spectral density profiles (panel a), open symbols are determined from numerical inversion of fixed-field data. The dashed line shows the temperature dependence of the proton dynamics for a classical, Arrhenius process. (b) – right axis: Spectral density amplitude $C_D K(T)$.***

Field dependent profiles of the spin-lattice relaxation rate provide a direct mapping of the spectral density, Eqn. (1). The magnetic field dependence of the $^1$H spin-lattice relaxation rate is presented in Figure 3a where $1/T_1^{(H)}(B_0)_T$ is plotted for seven temperatures in the range 0.1 < $B_O$ < 2.2 T. At the three lowest temperatures, 71.3 K, 76.9 K and 83.3 K the $1/T_1^{(H)}(B_0)_T$ curves are almost parallel, differing mainly in amplitude. This indicates that the inverse correlation time $\tau_c^{-1}$ is almost independent of temperature in this region. At 90.9 K, the spectral density begins to broaden indicating $\tau_c^{-1}$ is increasing. This trend progresses with increasing temperature up to 125 K and 142.9 K, when the curves appear almost parallel, indicating that $\tau_c^{-1}$ is once again independent of temperature.

The dependence of $\tau_c^{-1}$ at low temperature in Figure 3b, extracted from the fits in Figure 3a and inverting the fixed field $T_1$ data, **clearly** demonstrates proton tunnelling in this very short HB. At $T$ < **77** K, $\tau_c^{-1}$ is virtually independent of temperature, levelling off at $\tau_c^{-1} \approx 8\text{x}10^7$ s$^{-1}$, while below 91 K there is a clear deviation from the temperature dependence of a classical, Arrhenius process.

At higher temperature the apparent dynamical rate saturates above 110 K whereas it could be expected to continue to increase given that diffraction [40], NQR [50] and vibrational spectroscopy [51] report the cross-over from donor to acceptor species at 200K. Similarly, the temperature dependence of the spectral density amplitude (Figure 3b) shows a clear maximum at 105 K. In the usual model [21], in which all HB protons are assumed to have the same $\tau_c$, $K(T) = p(N).p(O)$ where $p(N)$ and $p(O)$ are the probabilities of the two states of the HB. The maximum of $K(T)$ should occur when $p(N) = p(O)$ and the observation of this condition at 105 K is therefore at odds with the experimental observations of the cross-over from donor to acceptor species i.e. $p(N) = p(O)$ at 200 K. This behaviour of the dynamical rate and the spectral density amplitude above 100K is due to the formation of N···HO domains.

In order to provide a model consistent with experimental data, we postulate that proton dynamics are effectively quenched in the thermodynamically stable high temperature N···HO phase and only the NH···O phase contributes to the NMR signal measured in the temperature range up to 140 K. The temperature dependence of the phase fractions is evaluated within a 1D Ising model [52] in which the NH···O and N···HO HB's are treated as positive and negative unit spins respectively, i.e. PT equates to inverting one spin.

The ground state depends on the sign of the coupling term *J*: a 'ferro' ground state, pure NH···O or N···HO domains, is obtained for $J<0$. An energy bias $B<0$ favours the NH···O ground state. The energy of this system of *n* spins is described by the equation

$$E = \sum_i^n (Js_i . s_{i+1} + Bs_i) \ where \ s = \pm 1 \quad (2)$$

The energy cost of inverting a single spin and thus creating a pair of domain walls equals $2B+4J$. The transfer HOXN···**H**OXNH → HOXN**H**···OXNH (X represents the rest of the molecule) must involve an energy difference equal to the transfer OXN···**H**OXN → OXN**H**···OXN as both transfers increase a NH···O domain by one unit. The same applies for the transfers OXN**H**···OXN → OXN···**H**OXN and HOXN**H**···OXNH → HOXN···**H**OXNH, which increase N···HO domains by one unit, but the energy difference in this case is opposite in sign. Two parameters are therefore sufficient to describe the system. The main adjustment with respect to the Ising model is the number of sites involved in domain walls, as a single PT from NH···O to N···HO in a pure domain of NH···O bonds creates a deprotonated molecule and a bi-protonated molecule, OXN···HOXNH, which are likely to affect the two neighbouring HB's.

Eqn. (2) is solved in a Monte Carlo simulation to analyse the domain and domain wall ($DW$) populations. The system evolves due to thermal fluctuations towards an equal mixture of N···HO and NH···O ('paramagnetic' state) at a temperature which depends on $B$ and $J$. In order to drive the system from NH···O towards N···HO, the energy bias $B$ is inverted linearly with temperature such that $B=0$ at 200 K, which is the temperature at which the cross-over from NH···O to N···HO species occurs. The extent to which $B$ goes negative determines how strongly the N···HO state is stabilised in competition with thermal fluctuations. The temperature range of interest here however is below 200 K with a view to understanding why the maximum in the spectral density amplitude occurs at 105 K.

Figure 4 shows the behaviour for an energy bias of $B$=-100 K and a coupling of $J$ = -20 K, giving the energy cost $A(T) \ (=-2B(T)-2J)$ of 280 K for transferring one proton at low temperature (0 K), which is in good agreement with that obtained from DFT calculations (Fig 2): $A$ = 285 K of which 27% is estimated to be due to coupling. $p(N)$ decreases from 1 to 0.5 at 200 K and the product $p(N).p(O)$ reaches a maximum at 200 K. In order for the maximum in the spectral density amplitude to be shifted to a temperature lower than 200 K, we have reasoned that only the NH···O phase, $p(N)$, is observed in the experiment. Figure 4 therefore shows the normalised product $p(N).[p(N).p(O)]$ which has a broad maximum at 140K, compared to 200K.

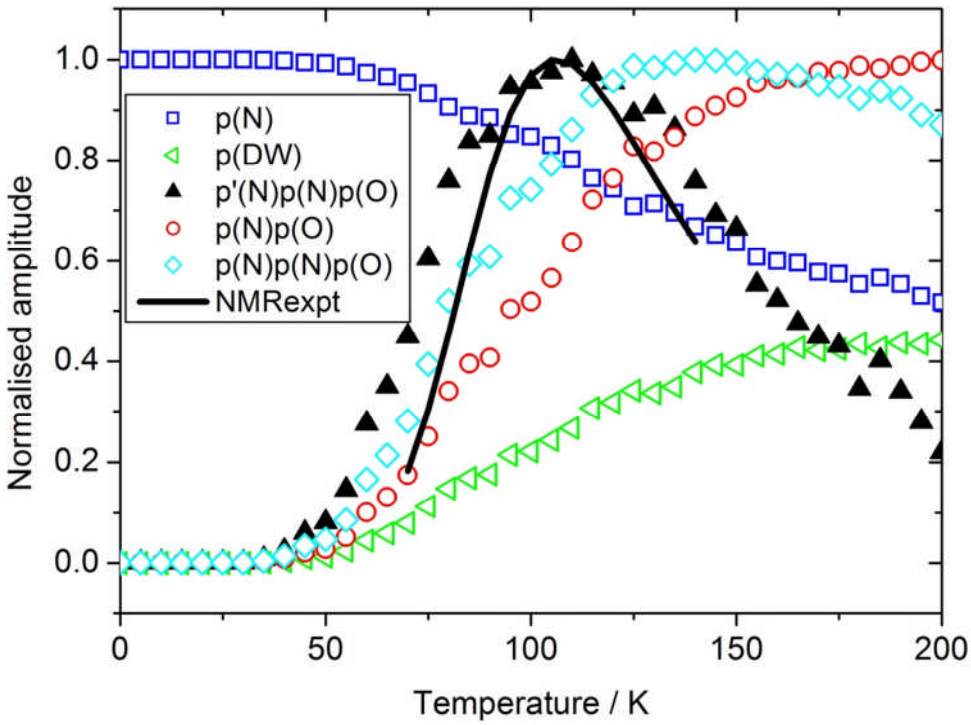


*Figure 4: Normalised amplitudes from the Ising model showing the switch-over in NH···O and N···HO populations at 200 K and the corresponding products of populations (p(N), p(O)) and domain walls (DW) relating to the function K(T) of Eqn. (1) (p'N=p(N)-p(DW)).*

The strength of *J* determines the size of domains that persist as temperature increases. In the case shown in Figure 4, the domain walls constitute ~40% of the system at 200 K and the average domain size is 2-3 HB's. Assuming that the domain walls also do not contribute to the spectral density, and therefore removing a minimal domain wall thickness of one spin, the product $(p(N)-p(DW)).[p(N).p(O)]$ is a more sharply-peaked function with a maximum just above 100 K, which agrees reasonably well with the experimental data [37].

The NMR data presented here demonstrates clearly that proton tunnelling occurs in 35PDCA in one of the shortest known N-H···O bonds and that the proton dynamics are non-classical up to 91 K. A 2D PES has been estimated from crystallographically determined structures for the deuterated crystal, which shows a low barrier between the donor and acceptor sites. Tunnelling through the barrier occurs because the effective mass of the tunnelling particle is high due to the displacement of the molecular skeleton during PT.

This work suggests that proton tunnelling occurs in all HB's and that tunnelling cannot be ignored as a PT mechanism in short, low-barrier HB's. Whether proton tunnelling in short HB's plays a

functional role at higher temperature, for example in enzyme catalysis, requires a precise evaluation of the cross-over temperature from quantum to classical dynamics.


[1] T.S. Moore, T.F. Winmill, *J. Chem. Soc.* **101**, 1635 (1912)
[2] W.M. Xu, E. Greenberg, G.K. Rozenberg, M.P. Pasternak, E. Bykova, T. Boffa-Ballaran, L. Dubrovinsky, V. Prakapenka, M. Hanfland, O.Y. Velikova, S.I. Simak, I.A. Abrikosov, *Phys. Rev. Letts.* **111**, 175501 (2013)
[3] T. Steiner, *Angew. Chem. Int. Ed.* **41**, 48 (2002)
[4] S.J. Grabowski, *Chem. Rev.* **111**, 2597 (2011)
[5] M. Meot-Ner, *Chem. Rev.* **112**, 22 (2012)
[6] *Isotope Effects in Chemistry and Biology*; Kohen, A., Limbach, H-H., Eds; CRC Press: Florida, 2006
[7] W.W. Cleland, M.M. Kreevoy, *Science* **264**, 1887 (1994)
[8] P.J. Guthrie, *Chemistry & Biology* **3**, 163 (1996)
[9] J.A. Gerlt, M.M. Kreevoy, W.W. Cleland, P.A. Frey, *Chemistry & Biology* **4**, 259 (1997)
[10] C.L. Perrin, *Acc. Chem. Res*. **43**, 1550 (2010)
[11] J. Trylska, P. Grochowski, J.A. McCammon, *Protein Sci.* **13**, 513 (2004)
[12] A. Langkilde, S.M. Kristensen, L.L. Leggio, A. Mølgaard, J.H. Jensen, A.R. Houk, J-C.N. Poulsen, S. Kauppinen, S. Larsen, *Acta Cryst.* **D64** (2008) 851–863
[13] M.J. Knapp, K. Rickert, J.P. Klinman, *J. Am. Chem. Soc.* **124**, 3865 (2002)
[14] L. Masgrau, A. Roujeinikova, L.O. Johannissen, P. Hothi, J. Basran, K.E. Ranaghan, A.J. Mulholland, M.J. Sutcliffe, N.S. Scrutton, D. Leys, *Science* **312** 237 ( 2006)
[15] M. Gil, J. Waluk, *J. Am. Chem. Soc.* **129**, 1335 (2007)
[16] V.A. Benderskii, E.V. Vetoshkin, I.S. Igribaeva, H.P. Trommsdorff, *Chem. Phys.* **262**, 393 (2000)
[17] Z. Smederchina, W. Siebrand, A. Fernandez-Ramos, *J. Chem. Phys.* **127**, 174513 (2007)
[18] C.R. Pudney, A. Guerriero, N.J. Baxter, L.O. Johannissen, J.P. Waltho, S. Hay, N.S. Scrutton, *J. Am. Chem. Soc.* **135**, 2512 (2013)
[19] J. Skinner, H.P. Trommsdorff, *J. Chem. Phys.* **89** 897 (1988)
[20] B. Schiøtt, B.B. Iversen, G.K.H. Madsen, T.C. Bruice, *J. Am. Chem. Soc.* **120** 12117 (1998)
[21] M. Neumann, D.F. Brougham, C.J. McGloin, M.R. Johnson, A.J. Horsewill, H.P. Trommsdorff, *J. Chem. Phys.* **109**, 7300 (1998)
[22] A. Oppenländer, Ch. Rambaud, H.P. Trommsdorff, J.C. Vial, Phys. Rev. Letters, **63** 1432 (1989)
[23] S. Nagaoka, N. Hirota, *Chem. Phys. Lett.* **92** 498 (1982)
[24] S. N. Smirnov, N.S. Golubev, G.S. Denisov, H. Benedict, P. Schah-Mohammedi, H.H. Limbach, *J. Am. Chem. Soc.* **118** 4094 (1996)
[25] A.O.F. Jones, M.H. Lemee-Cailleau, D.M.S. Martins, G.J. McIntyre, I.D.H. Oswald, C.R. Pulham, C.K Spanswick, L.H. Thomas, C.C. Wilson, *Phys. Chem. Chem. Phys.* **14**, 13273 (2012)
[26] T. Steiner, I. Majerz, C.C. Wilson, *Angew. Chem. Int. Ed.* **40**, 2651 (2001)
[27] C.C. Wilson, *Acta Crystallogr., Sect. B* **57**, 435 (2001)
[28] C.L. Perrin, J.S. Lau, Y.J. Kim, P. Karri, C. Moore, A.L. Rheingold, *J. Am. Chem. Soc.* **131** 13548 (2009)
[29] G. Pirc, J. Stare, J. Mavri, *J. Chem.Phys.* **132**, 224506 (2010)
[30] J. Sørensen, H.F. Clausen, R.D. Poulsen, J. Overgaard, B. Schiøtt, *J. Phys. Chem. A* **111** 345 (2007)
[31] S. Kong, I.G. Shenderovich, M.V. Vener, *J. Phys. Chem. A* **114** 2393 (2010)
[32] S.J. Grabowski, J.M. Ugalde, *Chem. Phys. Lett.* **493** 37 (2010)
[33] J. Chen, M.A. McAllister, J.K. Lee, K.N. Houk, *J. Org. Chem.* **63** 4611 (1998)
[34] C.A. Morrison, M.M. Siddick, P.J. Camp, C.C. Wilson, *J.Am. Chem. Soc.* **127**, 4042 (2005)

[35] F. Fontaine-Vive, M.R. Johnson, G.J. Kearley, J.A.K. Howard, S.F. Parker, *J. Am. Chem. Soc.* **128**, 2963 (2006)
[36] F. Fontaine-Vive, M.R. Johnson, G.J. Kearley, J.A. Cowan, J.A.K. Howard, S.F. Parker, *J. Chem. Phys.* **124**, 234503 (2006)
[37] See Supplemental Material [URL]
[38] F. H. Allen, *Acta Crystallogr. Sect. B.*, **58**, 380 (2002)
[39] J.A. Cowan, J.A.K. Howard, G.J. McIntyre, S.M.F. Lo, I.D. Williams, *Acta Crystallogr., Sect B* **59**, 794 (2003)
[40] S.J. Ford, O.J. Delamore, J.S.O. Evans, G.J. McIntyre, M.R. Johnson, I.R. Evans, *Chem. Eur. J.* **17**, 14942 (2011)
[41] B. Delley, *J. Chem. Phys.* **113**, 7756 (2000)
[42] G. Kresse, J. Hafner, *Phys. Rev. B*, **47**, 558 (1993)
[43] J.P. Perdew, K. Burke, M. Enzerhof, *Phys. Rev. Lett.* **78**, 1396 (1997)
[44] E.R. Andrew, L. Latanowicz, *J. Magn. Reson.* **68** 232 (1986)
[45] B.H. Meier, F. Graf, R.R. Ernst, *J. Chem. Phys.* **76** 767 (1982)
[46] Q. Xue, A.J. Horsewill, M.R. Johnson, H.P. Trommsdorff, *J. Chem. Phys.* **120** 11107 (2004)
[47] D. Brougham, A.J. Horsewill and H.P. Trommsdorff, *Chem. Phys.* **243** 189 (1999)
[48] A.J. Horsewill, *Progr. Nucl. Magn. Reson. Spectrosc* **52** 170 (2008)
[49] W. Wu, D.L. Noble, J.R. Owers-Bradley, A.J. Horsewill *J. Magn. Reson.* **175** 210 (2005)
[50] J. Seliger, V. Zagar, *J. Phys. Chem. A* **115**, 11652 (2011)
[51] S.J. Ford, Ph.D. Thesis, University of Durham, Durham, U.K., (2011)
[52] E. Ising, *Z. Phys* **31**, 253 (1925)

# PROTON TUNNELLING IN SHORT HYDROGEN BONDS

I. Frantsuzov[†,‡], S.J. Ford[#,ζ], I. Radosavljevic Evans[ζ], A.J. Horsewill[‡], H.P. Trommsdorff [#,ϒ], M.R. Johnson[#]

[‡]Department of Physics and Astronomy, University of Nottingham, Nottingham NG7 2RD, U.K.

[#]Institute Laue Langevin, BP 156, 38042 Grenoble, France

[ζ]Department of Chemistry, Durham University, Durham DH1 3LE, U.K.

[ϒ]University of Grenoble 1/CNRS, LIPhy UMR 5588, BP 87, 38041 Grenoble, France

## Supplementary Material

## *Histograms of O-H···O and N-H···O hydrogen bond lengths*

The distribution of donor-acceptor bond lengths for O-H···O and N-H···O hydrogen bonds, obtained from a database study of the compounds in the Cambridge Structure Database [1] is given in Figure 1. In this survey, simple O-H···O and N-H···O fragments were searched, with the non-bonded O···O and O···N distances defined as contacts. Furthermore the searches were constrained to find only organic, single crystal structures in which 3D coordinates had been determined and no disorder was present. The histograms given in Figure 1 show the frequency of hydrogen bond lengths for O···O and O···N hydrogen bonds and it can be seen that short hydrogen bonds, those with donor-acceptor distances of less than approximately 2.50 Å for O-H···O and 2.56 Å for N-H···O, are rare. The N···O distance in 35PDCA, the subject of this letter, is 2.54 Å, making it one of the shortest N-H···O hydrogen bonds. The O···O distance in benzoic acid, which has been studied extensively by NMR relaxometry and spin-lattice relaxation techniques, is 2.65 Å, making it an 'intermediate' length O-H···O hydrogen bond.

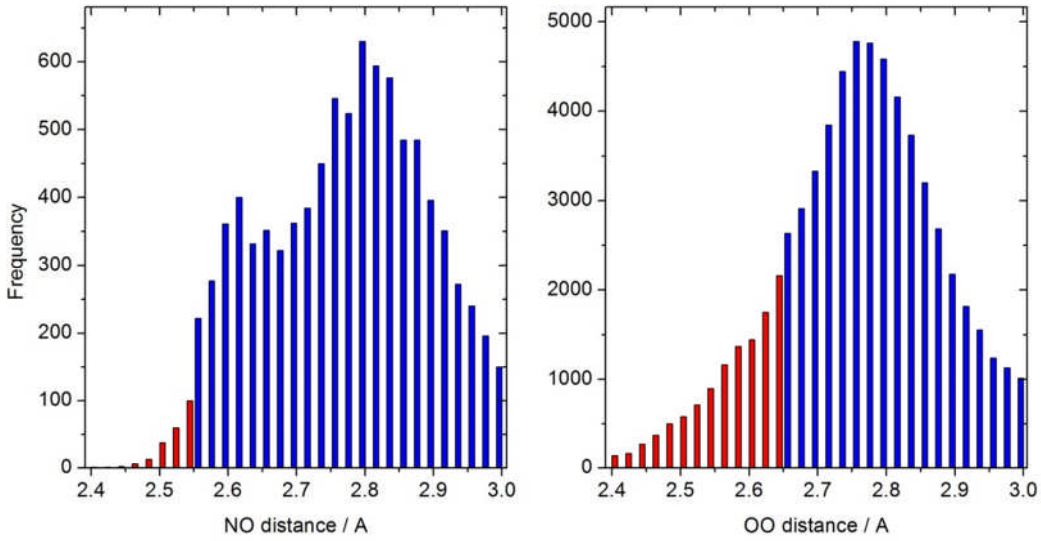


*Figure 1: Histograms of hydrogen bond lengths for (left) N-H···O and (right) O-H···O hydrogen bonds. The red columns indicate the hydrogen bonds shorter than (left) the N-H···O hydrogen bond in 35PDCA and (right) the O-H···O hydrogen bond in benzoic acid.*

## *Density functional theory methods and mapping of the two-dimensional potential energy surface*

A range of DFT calculations has been performed using the Dmol3 code [2]. In contrast to the VASP code used in previous work [3], which uses a plane-wave basis set for the electron density, Dmol3 uses a basis set of localised, numerical functions. The main reason for using Dmol3 was that it allowed the high temperature structure of 35PDCA,

with the proton transferred to the oxygen acceptor site, to be stabilised and thereafter a TS search to be performed, which was more difficult to achieve with plane-wave codes. Normal mode vibration calculations with Dmol3 have already been published for 35PDCA.

All Dmol3 calculations were performed at the same precision using the GGA-PBE [4] functional for consistency with previous calculations. The basis functions were double numerical with polarisation, with a global orbital cut-off of 3.7 Å, and the k-point grid was (3,2,4). All results were converged with respect to the choice of basis functions and k-point spacing. The energy tolerance for SCF cycles was $4x10^{-8}$ eV. For geometry optimisation the tolerance for energy change with respect to atomic coordinates was $4x10^{-7}$ eV and maximum residual force was $8x10^{-5}$ eV/Å.

Dmol3 was used to calculate the 2D potential energy surface (PES) for proton transfer accompanied by the displacement of the molecular skeleton (Figure 2). Linear interpolation between the extreme 'low' and 'high' temperature structures, after rescaling the low temperature cell parameters to those of the room temperature crystal structure and optimising the internal atomic coordinates, generated 10 structures. The 2D PES was obtained by calculating the energy of each of these structures while displacing the protons simultaneously along the 4 hydrogen bonds.

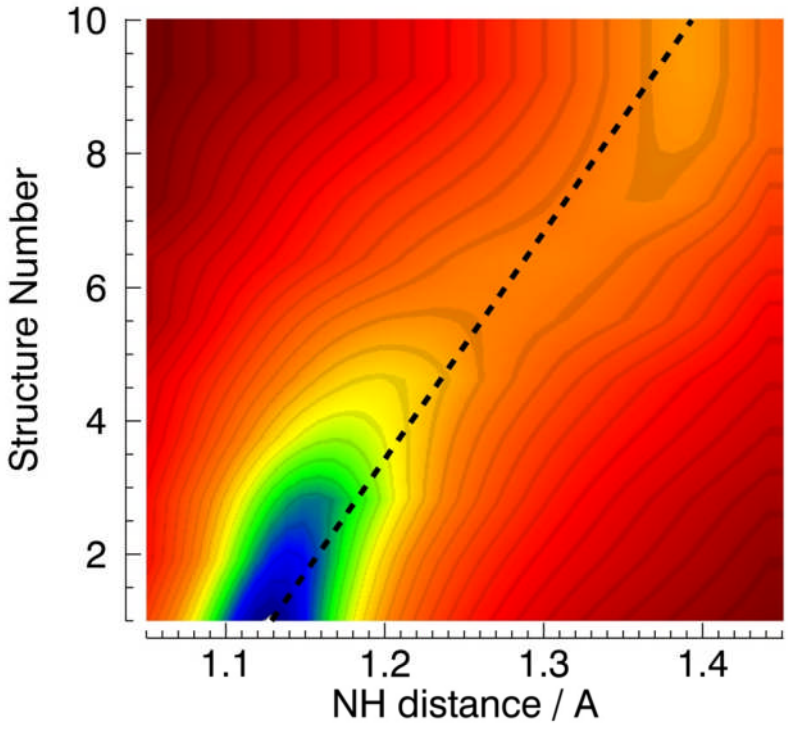

*Figure 2: 2D potential energy surface calculated as a function of the proton coordinate (X) and the skeletal displacement (Y). The dashed line shows the straight line path between the extreme 'low' (1) and 'high' (10) temperature structures.*

## *Single crystal sample preparation*

The 35PDCA sample was a single crystal and, for the spin-lattice relaxation measurements, was oriented so that the *c** crystal axis was aligned parallel with the applied static magnetic field. The crystals were grown using 3,5-pyridinedicarboxylic acid (Sigma–Aldrich, 98%), under hydrothermal conditions by using a 23 mL Parr general purpose acid digestion bomb (P/N 4749, Scientific & Medical Products), which consists of a Teflon reaction vessel inside a steel autoclave. Large cream-coloured crystals were obtained by heating 35PDCA (0.5 g) in $H_2O$ (7.5 mL) for 2 h at 200 $^{o}$C under pressure in the autoclave and cooling at a rate of 5 $^{o}$/min.

## *Spin-lattice relaxation equations*

In the 35PDCA system the modulation of the dipolar interactions dominates. The homonuclear and heteronuclear spectral density functions have been evaluated in the literature [5,6,7] and the spin-lattice relaxation equations pertaining to single crystal samples are summarised in references [7,8]. We define $\langle I_z \rangle$ and $\langle S_z \rangle$ as the longitudinal polarisations of the $^{1}$H and $^{14}$N spin systems with spin $I = \frac{1}{2}$ and $S = 1$ respectively. The spin-lattice relaxation behaviour is determined by the following coupled equations of motion,

$$\begin{bmatrix} \frac{d}{dt}\langle I_z \rangle \\ \frac{d}{dt}\langle S_z \rangle \end{bmatrix} = -\begin{bmatrix} \rho_{II} & \sigma_{IS} \\ \sigma_{SI} & \rho_{SS} \end{bmatrix} \begin{bmatrix} (\langle I_z \rangle - I_0) \\ (\langle S_z \rangle - S_0) \end{bmatrix} \qquad (1)$$

where $I_0$ and $S_0$ are the respective equilibrium polarisations and the elements of the relaxation matrix,

$$\mathbf{R} = \begin{pmatrix} \rho_{II} & \sigma_{IS} \\ \sigma_{SI} & \rho_{SS} \end{pmatrix} \qquad (2)$$

are spin-lattice relaxation rate expressions that sample the spectral density at the Larmor frequencies of the two nuclei, $\omega_H$ and $\omega_N$, and sums and differences of these

frequencies. For a single crystal sample the elements of the relaxation matrix are given by the following [7];

$$\rho_{II} = \frac{\gamma_H^2\gamma_N^2\hbar^2 S(S+1)}{6N_I}\frac{a}{(1+a)^2}\left(G_{Het}^0 L(\omega_H-\omega_N)+18G_{Het}^1 L(\omega_H)+9G_{Het}^2 L(\omega_H+\omega_N)\right)\left(\frac{\mu_0}{4\pi}\right)^2$$
$$+\frac{6\gamma_H^4\hbar^2 I(I+1)}{N_I}\frac{a}{(1+a)^2}\left[G_{Homo}^1 L(\omega_H)+G_{Homo}^2 L(2\omega_H)\right]\left(\frac{\mu_0}{4\pi}\right)^2$$

$$\sigma_{IS} = \frac{\gamma_H^2\gamma_N^2\hbar^2 I(I+1)}{6}\frac{a}{(1+a)^2}\left(-G_{Het}^0 L(\omega_H-\omega_N)+9G_{Het}^2 L(\omega_H+\omega_N)\right)\left(\frac{\mu_0}{4\pi}\right)^2$$
$$\sigma_{SI} = \frac{\gamma_H^2\gamma_N^2\hbar^2 S(S+1)}{6}\frac{a}{(1+a)^2}\left(-G_{Het}^0 L(\omega_N-\omega_H)+9G_{Het}^2 L(\omega_N+\omega_H)\right)\left(\frac{\mu_0}{4\pi}\right)^2 \quad (3)$$
$$\rho_{SS} = \frac{\gamma_H^2\gamma_N^2\hbar^2 I(I+1)}{6}\frac{a}{(1+a)^2}\left(G_{Het}^0 L(\omega_N-\omega_H)+18G_{Het}^1 L(\omega_N)+9G_{Het}^2 L(\omega_N+\omega_H)\right)\left(\frac{\mu_0}{4\pi}\right)^2$$

$\gamma_H$ is the $^1$H magnetogyric ratio so that in the static magnetic field $B_0$, the $^1$H Larmor frequency is $\omega_H = \gamma_H B_0$. $\gamma_N$ is the $^{14}$N magnetogyric ratio. The function $L(\omega) = 2\tau_c/(1+\omega^2\tau_c^2)$ is a Lorentzian with half-width at half-maximum equal to $\tau_c^{-1}$. There is efficient spin diffusion within the $^1$H reservoir so that a relaxation pathway involving a $^1$H nucleus becomes less efficient when the relaxation is shared among the total number of hydrogen nuclei in the molecule: in the 35PDCA molecule $N_I = 5$ is the number of $^1$H nuclei for each mobile $^1$H nucleus.

The factor $a/(1+a)^2$ is determined by the statistical thermodynamic properties of the system and the normalised product of the populations of the two sites *N (=a)* and *O (=1)*. In a static two-well potential with potential energy asymmetry *A*, $a = exp(A/kT)$. More generally, $A$ would be replaced by the free energy $\Delta G = A - T\Delta S$ which allows the free energy, two-well potential to be inverted with increasing temperature.

In Eqn.(3), $\rho_{II}$ comprises two terms, the first arises from $^{14}$N-$^1$H heteronuclear interactions and the second from $^1$H-$^1$H homonuclear interactions. The relative magnitude of these two will later determine the data analysis procedures adopted. $G_{Het}^i$ and $G_{Homo}^i$ are lattice sums determined by the geometries of the $^{14}$N-$^1$H (heteronuclear) and $^1$H-$^1$H (homonuclear) internuclear vectors respectively and their orientation with respect to the axis of $B_0$ as follows, [7]

$$
\begin{aligned}
G^0_{Het} &= \sum_{i,k}\left[ r_{ikA}^{-3}\left(1-3\cos^2\theta_{ikA}\right)+r_{ikB}^{-3}\left(1-3\cos^2\theta_{ikB}\right)\right]^2 \\
G^1_{Het} &= \sum_{i,k}\left[\begin{array}{l} r_{ikA}^{-6}\sin^2\theta_{ikA}\cos^2\theta_{ikA}+r_{ikB}^{-6}\sin^2\theta_{ikB}\cos^2\theta_{ikB} \\ -2r_{ikA}^{-3}r_{ikB}^{-3}\cos\theta_{ikA}\cos\theta_{ikB}\left(\cos\alpha-\cos\theta_{ikA}\cos\theta_{ikB}\right)\end{array}\right] \\
G^2_{Het} &= \sum_{i,k}\left[\begin{array}{l} r_{ikA}^{-6}\sin^4\theta_{ikA}+r_{ikB}^{-6}\sin^4\theta_{ikB} \\ -4r_{ikA}^{-3}r_{ikB}^{-3}\left(\cos\alpha-\cos\theta_{ikA}\cos\theta_{ikB}\right)^2+2r_{ikA}^{-3}r_{ikB}^{-3}\sin^2\theta_{ikA}\sin^2\theta_{ikB}\end{array}\right] \\
G^1_{Homo} &= \sum_{j\neq k}\left[\begin{array}{l} r_{jkA}^{-6}\sin^2\theta_{jkA}\cos^2\theta_{jkA}+r_{jkB}^{-6}\sin^2\theta_{jkB}\cos^2\theta_{jkB} \\ -2r_{jkA}^{-3}r_{jkB}^{-3}\cos\theta_{jkA}\cos\theta_{jkB}\left(\cos\alpha-\cos\theta_{jkA}\cos\theta_{jkB}\right)\end{array}\right] \\
G^2_{Homo} &= \sum_{j\neq k}\left[\begin{array}{l} r_{jkA}^{-6}\sin^4\theta_{jkA}+r_{jkB}^{-6}\sin^4\theta_{jkB} \\ -4r_{jkA}^{-3}r_{jkB}^{-3}\left(\cos\alpha-\cos\theta_{jkA}\cos\theta_{jkB}\right)^2+2r_{jkA}^{-3}r_{jkB}^{-3}\sin^2\theta_{jkA}\sin^2\theta_{jkB}\end{array}\right]
\end{aligned}
\qquad (4)
$$

$k$ labels the hydrogen bond proton, $i$ the nitrogen and $j$ a second proton. The dipolar contribution from a nucleus labelled $i$ or $j$ interacting with proton $k$ is defined by an internuclear vector with length $r$ which subtends an angle $\theta$ with respect to the applied magnetic field. The internuclear vector can adopt either configuration $A$ or $B$ depending on the site adopted by the proton in the hydrogen bond. The angle $\alpha$ is the angle subtended by the two internuclear vectors in configurations $A$ and $B$. If the sums in Eqn. (4) are confined to the immediate vicinity of the SSHB in one molecule, the system comprises just one N-H heteronuclear interaction and two homonuclear interactions between the SSHB proton and the two phenyl protons; in that case $G^i_{Het}$ contains one term in the summation and $G^i_{Homo}$ contains two.

That deviations from single exponential recovery were rather small enables us to make certain approximations. The $^{14}$N magnetogyric ratio is approximately 14 times smaller than that of $^1$H so that $\omega_N$ is small compared with $\omega_H$. As a result, the Lorentzian functions $L\left(\omega_H+\omega_N\right)$ and $L\left(\omega_H-\omega_N\right)$ approximate to $L\left(\omega_H\right)$. Further, in support of the experimental observations, numerical modelling of the spectral density terms based on the crystal structure [9] shows that the $^1$H spin-lattice relaxation is closely approximated by the diagonal element of the relaxation matrix. Therefore, we may approximate the $^1$H magnetisation evolution by

$$\frac{d}{dt}\left\langle I_z\right\rangle = -\rho_{II}\left[\left\langle I_z\right\rangle - I_0\right]$$

and the effective relaxation rate in a polarisation-recovery experiment is given by

$$1/T_1^{(H)} \approx \rho_{II}$$

Applying these approximations, the diagonal element $\rho_{II}$ governing the spin-lattice relaxation of the $^1$H reservoir (Eqn. (3)) may be written;

$$\begin{aligned}\rho_{II}(\omega_H) &\approx \frac{a}{(1+a)^2}[(P_{Het}G^0_{Het} + 18P_{Het}G^1_{Het} + 9P_{Het}G^2_{Het} + P_{Homo}G^1_{Homo})L(\omega_H) \\ &\quad + P_{Homo}G^2_{Homo}L(2\omega_H)] \\ &\approx \frac{a}{(1+a)^2}[C_1L(\omega_H) + C_2L(2\omega_H)] \\ &\approx C_D\frac{a}{(1+a)^2}[cL(\omega_H) + (1-c)L(2\omega_H)] \qquad (5)\end{aligned}$$

where $C_D$ is a dipolar constant

$$C_D = \left(P_{Het}G^0_{Het} + 18P_{Het}G^1_{Het} + 9P_{Het}G^2_{Het} + P_{Homo}G^1_{Homo} + P_{Homo}G^2_{Homo}\right)$$

with $P_{Het} = \frac{\gamma_I^2\gamma_S^2\hbar^2}{15}\left(\frac{\mu_0}{4\pi}\right)^2$, $P_{Homo} = \frac{9\gamma_I^4\hbar^2}{10}\left(\frac{\mu_0}{4\pi}\right)^2$, and $0 \le c \le 1$ is the dimensionless constant, $c = \frac{C_1}{C_1 + C_2}$.

Therefore, Eqn. (5) may be used to analyse the experimental $1/T_1^{(H)}(B_0)$ profiles and extract the parameters that define the proton migration. There are two terms that characterise the temperature dependence of $1/T_1^{(H)}(B_0)$; the width of the spectral density depends on $\tau_c^{-1}(T)$ while the amplitude is governed by

$$K(T) = C_D\, a/(1+a)^2 = C_D \exp(\Delta G/k_BT)/(1+\exp(\Delta G/k_BT))^2 . \qquad (6)$$

This function has been used to fit the data in Figure 3b of the letter with $A$ = 613 K and $\Delta S$ = 5.22. This value of $A$ is twice as big as that estimated from DFT calculations (285 K) which constitutes a third reason for rejecting this simplistic model and developing the Ising model.

## *Fixed-field spin-lattice relaxation data*

The inverse temperature dependence of the $^1$H spin-lattice relaxation time recorded at $B_0$ = *0.864 T* ($\omega_H$ = *36.8 MHz)* is plotted in Fig. 3. A shallow minimum is observed at $T \approx 100$ *K* with $(T_1^{(H)})_{min} = 59$ *s*. Below 67 K ($1/T \approx 0.015$ $K^{-1}$), $^1$H spin-lattice relaxation becomes almost temperature independent with $T_1^{(H)} \approx 1000$ *s,* due to impurities, as has been observed in thioindigo-doped benzoic acid [10]. Above 170 K ($1/T \approx 0.006$ $K^{-1}$) $T_1^{(H)}$ becomes almost temperature independent at approximately 180 s, due to the formation of domains.

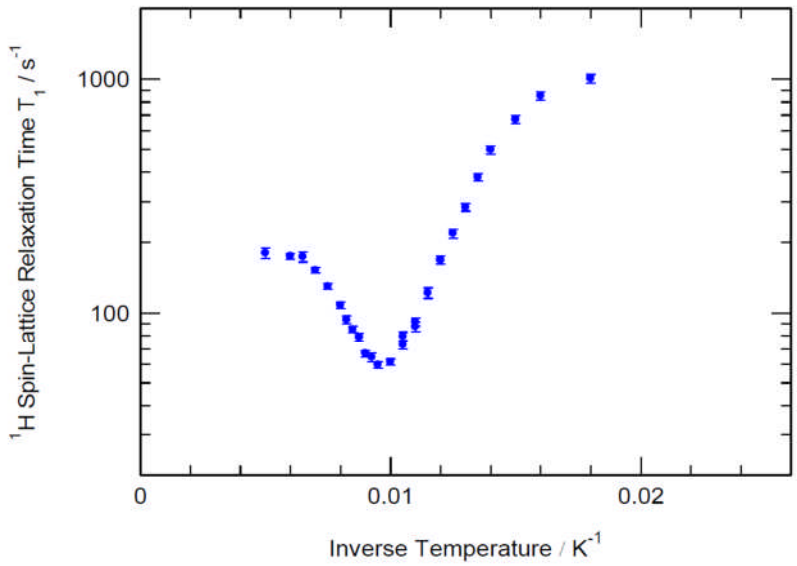


*Figure 3: The inverse temperature dependence of the $^1$H spin-lattice relaxation time in 35PDCA recorded at fixed field, $B_0$ = 0.864 T ($\omega_H$ = 36.8 MHz). The minimum is assigned to the proton transfer process.*

## *Ising model*

Additional results are shown for the Ising model to demonstrate the best match to experimental data for the energy bias parameter, *B*, with a value of -100 K and the coupling parameter, *J*, with a value of -20 K.

Figure 4 (top) shows the effect of varying *J* on the simulated spectral density amplitude. For a given energy cost of proton transfer *A*, increasing *J* increases the size of domains at a given temperature resulting in a slower decay of the intensity after the maximum. Increasing *J* also tends to move the onset of the increase in spectral density amplitude to higher temperature since, at low temperature, *B* and *J* have a similar effect in stabilising the ground state. However, in this model, *J* is constant whereas |*B*| decreases with increasing temperature.

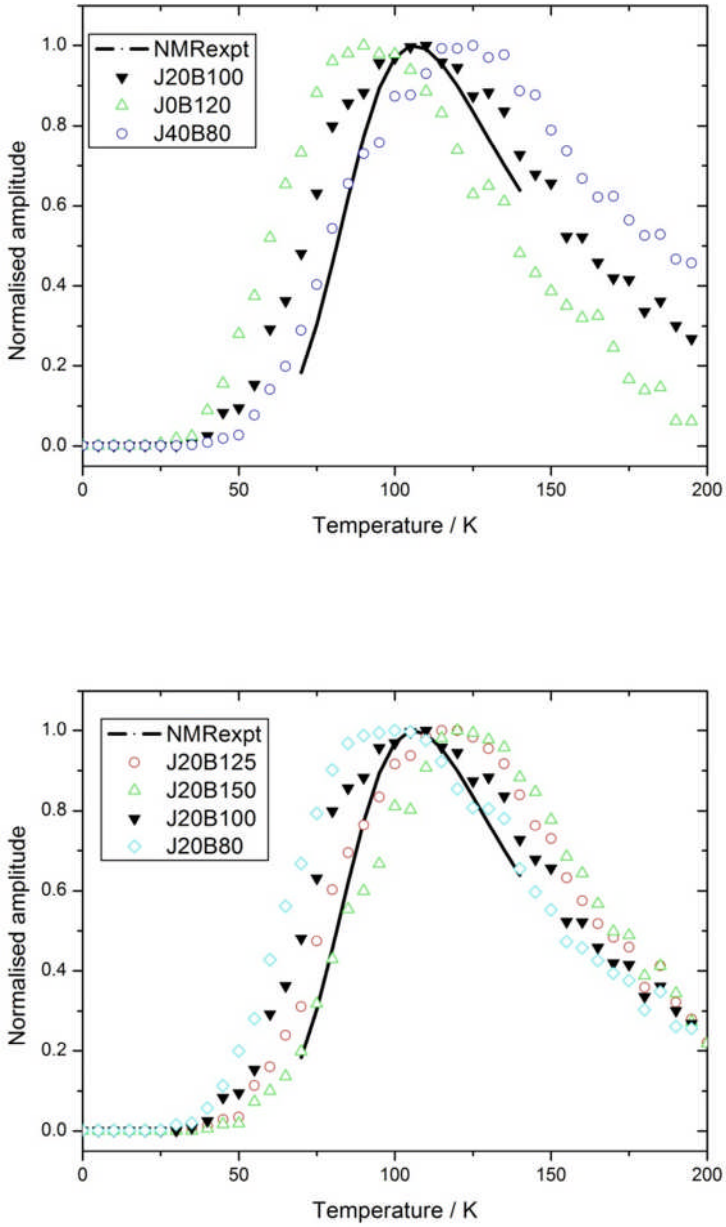


*Figure 4: (top) Effect of coupling -J ∈ {0, 20 ,40 K} and energy bias -B ∈ {120, 100, 80 K} for a fixed value of A(0) = 280 K on the calculated spectral density amplitude. (bottom) Effect of -B ∈ {80, 100, 125, 150 K} for a fixed value of -J = 20 K on the calculated spectral density amplitude.*

Figure 4 (bottom) shows the effect of increasing *B* for a given value of *J*. Again a bigger value of *B* moves the onset of the increase in the spectral density amplitude to higher temperature but it also increases the temperature of the maximum. Figure 4 demonstrates that the best, qualitative agreement with the experimental data is obtained for $|A|=280\ K$: $B= -100\ K$ and $J = -20\ K$.

[1] F. H. Allen, *Acta Crystallogr. Sect. B.*, **58**, 380 (2002)

[2] B. Delley, *J. Chem. Phys.* **113**, 7756 (2000)

[3] G. Kresse, J. Hafner, *Phys. Rev. B*, **47**, 558 (1993)

[4] J.P. Perdew, K. Burke, M. Enzerhof, *Phys. Rev. Lett.* **78**, 1396 (1997)

[5] E.R. Andrew and L. Latanowicz, *J. Magn. Reson.* **68** 232 (1986)

[6] B.H. Meier, F. Graf and R.R. Ernst, *J. Chem. Phys.* **76** 767 (1982)

[7] Q. Xue, A.J. Horsewill, M.R. Johnson, H.P. Trommsdorff, *J. Chem. Phys.* **120** 11107 (2004)

[8] A.J. Horsewill, *Progr. Nucl. Magn. Reson. Spectrosc.* **52** 170 (2008)

[9] J.A. Cowan, J.A.K. Howard, G.J. McIntyre, S.M.F. Lo, I.D. Williams, *Acta. Cryst. B* **61** 724730 (2005)

[10] D. Brougham, A.J. Horsewill, H.P. Trommsdorff, *Chem. Phys.* **243** 189 (1999)